Chemical Engineering Journal 489 (2024) 151308

Contents lists available at ScienceDirect

Chemical Engineering Journal

journal homepage: www.elsevier.com/locate/cej

Efficient degradation of naphthenic acids in water using a sustainable engineered biochar/ZnO composite under simulated solar light

Zhexuan An [a], Isaac Sánchez-Montes [a], Pamela Chelme-Ayala [a], Chunmao Chen [b], Mohamed Gamal El-Din [a,*]

[a] Department of Civil and Environmental Engineering, University of Alberta, T6G 1H9 Edmonton, AB, Canada
[b] State Key Laboratory of Petroleum Pollution Control, Beijing Key Laboratory of Oil and Gas Pollution Control, China University of Petroleum-Beijing, Beijing 102249, China

ARTICLE INFO

Keywords:
Naphthenic acids
Biochar supported photocatalyst
Zinc oxide
Solar degradation
Reactive oxygen species

ABSTRACT

Naphthenic acids (NAs) present in oil sands process water (OSPW) have brought increasing environmental concerns due to their potential risk to aquatic and mammalian species. In this study, sustainable biochar zinc oxide (BC/ZnO) composites were synthesized using wood waste with different ZnO content and applied under simulated solar light for the photocatalytic degradation of different NAs for the first time. The best experimental conditions were determined as 0.5 g/L BC/30%ZnO and 4 h of simulated solar irradiation time, achieving 93.7 % degradation of cyclohexanecarboxylic acid (CHA) following the pseudo-first order kinetics. BC, with a porous structure and roughened surface, acted as an excellent platform for ZnO particles and an electron reservoir to inhibit the recombination of photogenerated electron-hole pairs. Hydroxyl radicals ($^{\bullet}$OH) were identified to play the dominant role in CHA degradation, and the enhanced photocatalytic performance of the BC/30%ZnO composite was proved by more $^{\bullet}$OH species detected compared to synthesized ZnO. The composite showed good reusability and stability after 4 successive cycles of use, still achieving 92.9 % degradation of CHA. Moreover, this is the first study applying BC/30%ZnO composite for the simultaneous degradation of a complex mixture of eight NAs with significantly different chemical structures. The competition kinetics were observed among different NAs in the mixture, resulted in over 95 % degradation of total NAs after 6 h treatment. By applying wood waste-based BC/ZnO composite with excellent photocatalytic performance in combination with solar light as green energy source, this research highlights a promising sustainable approach for real OSPW remediation.

1. Introduction

Naphthenic acids (NAs) are recognized as a family of saturated aliphatic and alicyclic carboxylic acids that are naturally present in the oil sands in northern Alberta and other oil reserves [1,2]. During the bitumen extraction process, approximately every 1 m^3 of oil sand consumes about 2 to 3 m^3 of fresh water, leading to a large amount of production of oil sands process water with solubilized NAs. OSPW is stored in on-site tailings ponds, presenting challenges due to its continuous accumulation and potential environmental risks and requiring the development of new treatment alternatives to achieve its reclamation [1,3–5]. In fact, NAs in OSPW have brought environmental concerns since several studies have reported that these compounds could cause acute and chronic toxicity to aquatic and mammalian species [6–10].

NAs can be represented by the general formula $C_nH_{2n+z}O_x$, where “n” indicates the carbon number ($7 \leq n \leq 26$), “z” means the hydrogen deficiency due to the ring or double bond in the chemical structure of the acids (even integer, $0 \leq -Z \leq 18$), and “x” the oxygen number (typically $2 \leq x \leq 6$) [11]). Classical NAs could be typically characterized with an oxygen number equal to 2, and the oxidized NAs (Oxy-NAs) have an oxygen number ranging from 3 to 6. Furthermore, heteroatomic NAs could be represented as $C_nH_{2n+z}SO_x$ and $C_nH_{2n+z}NO_x$ [11]. In general, most studies have focused on the removal of classical NAs and oxy-NAs from OSPW; however, studying the degradation of heteroatomic NAs is also important and worth further investigation [12].

Conventionally, passive treatment methods for OSPW such as end pit lakes and constructed treatment wetlands require protracted hydraulic retention times and volumes to address the recalcitrance of NAs to achieve the remediation [13,14]. Advanced oxidation processes (AOPs)

---

* Corresponding author.
E-mail address: mgamalel-din@ualberta.ca (M. Gamal El-Din).

https://doi.org/10.1016/j.cej.2024.151308
Received 23 December 2023; Received in revised form 8 April 2024; Accepted 13 April 2024
Available online 16 April 2024

are promising treatment methods for the remediation of various matrices, including OSPW. Different AOPs have been applied for the degradation of natural and synthetic NAs, such as ozonation [15,16], sulfate radical-based processes [17], Fenton and Fenton-like systems [18,19], UV-based processes [20], among others. The degradation mechanism of these AOPs is based on the generation of highly reactive radicals, mainly hydroxyl ($^{\bullet}OH$), sulfate ($SO_4^{\bullet-}$), and superoxide ($O_2^{\bullet-}$) radicals, which can oxidize organic matter into shorter chain by-products. However, drawbacks such as the use of oxidizing agents and the high energy demand required for their operation have limited the application of these AOPs [21,22].

Semiconductor-assisted photocatalysis has emerged as a sustainable AOP due to its potential to generate radical and non-radical species in combination with solar energy [23,24]. Besides, solar-based photocatalysis has shown promise to be applied in combination with established OSPW treatment to achieve efficient and effective removal of NAs, for instance, solar photocatalytic reactors were recognized as a hybrid component with great potential in constructed wetland treatment systems [13]. Due to its effectiveness and low cost, zinc oxide (ZnO) has been proposed as a promising photocatalyst for water treatment; however, its relatively wide band gap (3.37 eV) and high exciton binding energy (60 meV) hinder its excitation under visible light [25]. Furthermore, the photocorrosion effect and the high recombination rate of photogenerated electron-hole (e^{-}-h^{+}) pairs are commonly reported as further disadvantages of ZnO [24,26].

Recently, biochar-supported photocatalysis has emerged as a new strategy to overcome the limitations of individual photocatalytic materials [27]. Loaded photocatalysts on biochar (BC) surfaces can produce composites with greater adsorption capacities, higher chemical stability, and enhanced photocatalytic degradation compared to bare semiconductor photocatalysts [27]. Cai et al. [25] prepared a novel BC/ZnO composite photocatalyst using pine as the carbon source and achieved effective degradation of metronidazole under visible light irradiation. Gonçalves et al. [28] synthesized BC/ZnO composites using biowaste from brewed coffee and chitosan. In that study, the photocatalytic performance of the composite for degrading solutions containing phenol was superior to that of pristine ZnO. Chen et al. [29] and Yang et al. [24] also reported that composites are beneficial to obtain better photocatalytic performance by muti-scale fine structures and excellent characteristics, more reactive sites, and the inhibition ability of the recombination rate of the photoinduced e^{-}-h^{+} pairs.

Although recent studies have proved the great potential of BC/ZnO composite as a photocatalyst, there remains a research gap in assessing the effectiveness and feasibility of this material for the solar degradation of OSPW-related NAs. Furthermore, despite OSPW typically containing hundreds (if not thousands) of NAs with diverse chemical structures, most of the studies have focused on the degradation of a single model or several NAs separately [12,30,31], lacking investigations into the correlation between the chemical structure of these compounds and the performance of the treatment. Herein, investigating the photocatalytic performance of the BC/ZnO composite in the degradation of a complex mixture simultaneously containing several NAs is valuable and essential to evaluate its potential application in real OSPW remediation.

Moreover, large amounts of wood waste are generated annually by forestry, agricultural, and energy/food industries [32]. Despite the potential for reuse as valuable biomass, much of this waste is disposed of in landfills, leading to wasted land resources and increased greenhouse gas emissions [33]. However, wood waste can serve as a low-cost raw material for producing biochar, offering a promising method for processing residual biomass from forestry [34].

This study aimed to develop sustainable wood-waste-based BC/ZnO composites and use them in combination with solar light for the effective photocatalytic degradation of several models of NAs. The photocatalytic performance of prepared BC/ZnO composites was expected to be enhanced compared to ZnO only, which was thoroughly studied through: 1) the effect of the ZnO content and the dosage of the composite on the degradation of a single model NA (cyclohexanecarboxylic acid, CHA), 2) the kinetics of the degradation of CHA, 3) the investigation of the main reactive oxygen species (ROS) generated during the photocatalytic process, and 4) the assessment of the reusability of the BC/ZnO composite in the best experimental conditions. Moreover, for the first time in the literature, the composite with the best ZnO content was applied to treat a complex mixture containing NAs with significant differences in their chemical structures, which could provide important insights into the potential treatment of real OSPW in future studies using this approach.

2. Materials and methods

2.1. Materials and reagents

Hardwood forestry wastes (Aspen wood) were used as biomass to prepare the pristine and BC/ZnO composites. The samples were provided by Inno Tech Alberta. The following chemicals were used without any further purification: zinc nitrate hexahydrate ($Zn(NO_3)_2\ 6H_2O$; Sigma Aldrich), anhydrous sodium carbonate (Na_2CO_3; Fisher Scientific), 5,5-dimethyl-1-pyrroline *N*-oxide (DMPO; Dojindo Laboratories), 5-*tert*-butoxycarbonyl 5-methyl-1-pyrroline *N*-oxide (BMPO; Dojindo Laboratories), 2,2,6,6-tetramethylpiperidine (TEMP; Fisher Scientific), and NAs models (cyclohexanecarboxylic acid (CHA), isonipecotic acid (IA), tetrahydro-2H-thiopyran-4-carboxylic acid (T-2H-T4CA), tetrahydropyran-4-carboxylic acid (T4CA), cyclohexanepentanoic acid (CHPA), hexanoic acid (HA), 4-methylheptanoic acid (4-MHA), and decanoic acid (DA); Sigma Aldrich). To simulate a pH similar to real OSPW (around 8.5), all NAs solutions were prepared in buffer using 5 mM sodium bicarbonate ($NaHCO_3$; Fisher Scientific). Ultrapure water (Millipore Synergy UV, $\rho \geq 18.2$ MΩ cm) was used to prepare all solutions.

2.2. Experimental methods

2.2.1. Synthesis of BC and BC/ZnO composites

First, hardwood wastes were dried in an oven at 105 °C overnight to remove the water content. Then, the dried raw material was submitted to pyrolysis using a muffle furnace (Lindberg/Blue M BF51894C-1, Thermo Scientific) at 600 °C (10 °C/min heating rate) for 2 h under N_2 atmosphere. The obtained material was cooled to room temperature and rinsed three times with ultrapure water, followed by a drying step at 105 °C. The product was finally sieved evenly and stored in dark glass bottles for future use. In this work, pristine biochar is referred to as BC.

The composites, i.e., BC/ZnO, were synthesized by impregnation method with the designed ZnO contents as 10, 20, 30, and 50% wt [35]. A certain amount of BC was dispersed in a certain volume of ultrapure water. Subsequently, a corresponding volume of $Zn(NO_3)_2$ stock solution (0.5 M) was added to the previous dispersion under continuous stirring. After 5 min, a certain volume of Na_2CO_3 stock solution (1 M) was added to the solution dropwisely under constant stirring. The final dispersion should reach 30 mL and the solution was stirred at room temperature for 1 h for the precipitation of zinc carbonate. Next, the solution was transferred to 50 mL Flacon tubes, and the solid products were separated by centrifugation (Centrifuge 5810 R, Eppendorf) at 5000 rpm for 5 min, washed with ultrapure water, and dried overnight at 80 °C. Finally, the dried material was calcined at 600 °C for 2 h (in N_2 environment) to yield the biochar/ZnO. For comparison, synthesized ZnO without biochar (Syn-ZnO) was produced by the same method without adding biochar. A scheme of the steps involved in the fabrication of the BC/ZnO composites can be seen in Fig. S1.

2.2.2. Characterization of the BC/ZnO

Various techniques were employed to characterize the best BC/ZnO composite: 1) the morphology and the chemical composition of the composite catalyst were investigated by scanning electron microscopy and energy-dispersive X-ray spectroscopy (SEM-EDX, Zeiss Sigma 300 VP-FESEM equipped with a Bruker EDX system); 2) the phase composition was identified by X-ray diffraction spectroscopy (XRD, Ultima IV, Rigaku, from 5° to 90°, CuKα_1 1.5406 Å, CuKα_2 1.5444, CuKβ 1.3922); 3) the surface chemical composition and chemical stats analysis were conducted by X-ray photoelectron spectroscopy (XPS, Kratos AXIS 165, Kratos Analytical); 4) the elemental analysis was performed by inductively coupled plasma-optical emission spectroscopy (ICP-OES, iCAP6300 Duo, Thermo); 5) the band gap and optical properties were analyzed by UV–Vis diffuse reflectance spectra (UV–VIS-NIR Cary 5000 with a DRA-CA-50 M accessory, Agilent) and the photoluminescence (PL) spectra (Fluorimeter QM-8075–11, HORIBA-PTI).

In addition, the point of zero charge (PZC) of the BC/ZnO composite was determined by the salt addition method previously reported in detail by Nguyen et al. [36] and Jang et al. [37]. In brief, the pH of a 0.01 M NaCl solution was adjusted to the pH range from 2 to 10 (initial pH = pH_0) using 0.1 M HCl or 0.1 M NaOH solutions. Next, 5 mg of the BC/ZnO composite was added to falcon tubes containing 25 mL of the pH-adjusted 0.01 M NaCl solution. To minimize the CO_2 effect, the tube was filled with nitrogen gas in the headspace and sealed, then, placed on a platform shaker at 150 rpm for 48 h. After the agitation period was completed, the equilibrium pH (final pH = pH_f) was measured and recorded. For each tube, the difference between the pH (ΔpH) values was calculated by the subtraction of pH_0 to the pH_f. Then, ΔpH vs. pH_0 was plotted, and PZC of the composite was determined when ΔpH = 0.

2.3. Photocatalytic degradation experiments

The photocatalytic performance of the BC/ZnO composites with different ZnO content was first investigated for the degradation of CHA (25 mg/L), a classical NA. 0.5 g/L of BC/ZnO composite was added to a cylindrical glass reactor containing a 60 mL solution of the targeted NA. Before irradiation, the suspension was stirred steadily at dark condition for 60 min to reach the adsorption-equilibrium process. Subsequently, the system was exposed to simulated solar irradiation (SS200AAA, Photon Emission Tech; 1000 W ozone-free arc lamp) under continuous stirring. A fixed irradiance of 100 mW/cm^2 was used for all the experiments. At certain intervals, samples were withdrawn from the reacting solution and filtered using 0.2 μm Nylon filters (Thermo Scientific). The filtered samples were stored in the fridge at 4 °C until further analyses. All experiments were conducted in duplicate. The setup used in the photocatalytic experiments is shown in Fig. S2.

2.4. ROS and reusability test

Electron paramagnetic resonance (EPR) analyses were employed to identify the main ROS that drive the degradation of CHA by the BC/ZnO composite. The analyses were conducted using an EPR spectrometer (ELEXSYS-II, Bruker E-500) with a center field and resonance frequency of 3897 G and 9.81 GHz, respectively. The EPR spectra were collected based on the set-up of magnetic field modulation, amplitude, microwave power as 100 kHz, 1.0 G, and 20 mW, with a sweep time of 60 s. The EPR experiments were performed in a 5 mL reactor using a 1 mL solution following the same experimental setup mentioned in Section 2.3. To load the sample into the EPR assembly for analysis, a 200 μL aliquot was withdrawn from the system and transferred to a Suprasil quartz tube with one end sealed and placed in a tripe tube cell. DMPO (50 mM) and BMPO (3 mM) were used as spin–trap reagents to detect $^{\bullet}OH$ and $O_2^{\bullet-}$ species, while TEMP (200 mM) was employed to detect the presence of singlet oxygen ($^1O_2$).

The stability and reusability of the BC/ZnO composite was investigated for the best ZnO content. For that, photocatalytic experiments for the degradation of CHA were repeated for four cycles. After each cycle, the used photocatalyst was separated from the treated solution by vacuum filtration. Then, the material was washed with ultrapure water three times and dried at 60 °C overnight for next cycle use.

2.5. Photocatalytic performance of the BC/ZnO composite in the degradation of a mixture of NAs

The photocatalytic degradation performance of the best BC/ZnO composite was investigated for the simultaneous degradation of eight NAs model compounds with significant differences in their chemical structures. The general properties of the NAs compounds are listed in Table 1. Based on previous studies working with real OSPW samples, the initial total NAs concentration was selected to be 40 mg/L (i.e., 5 mg/L of each NA in 5 mM $NaHCO_3$ buffer) [38,39]. To our knowledge, this is the first work to evaluate the degradation efficiency and the competition kinetics toward NAs mixture using a BC/ZnO composite with simulated solar irradiation, which could give an essential insight into the complicated relationship between the structure and the preferential degradation phenomenon of NAs. Considering the complex composition of NAs in real OSPW, the outcomes of this experiment would serve as proof of concept for the potential implementation of this composite material in the remediation of OSPW in the future.

Finally, the acute toxicity of both the untreated and treated NAs mixture solution was assessed using a Microtox® screening bioassay, a widely used method for evaluating acute toxicity with *Vibrio fischeri* (*V. fischeri*), a luminescent marine bacteria [38,40]. The *V. fischeri* suspension was exposed to the samples, with pH adjusted to 6.5–7.0, at 15 °C for 15 min. The luminescence intensity of the bacteria in 2 % NaCl in deionized water and in phenol solution was used as negative and positive controls, respectively. Luminescence intensity readings were taken at 0, 5, and 15 min using a microplate reader (BioTek Synergy H1 microplate) and the inhibition effect (%) was determined using the following equations:

$$R_t = \frac{I_{0-B}}{I_{t-B}} \tag{1}$$

$$G_{t-s} = \frac{I_{0-s} \times R_t}{I_{t-s}} - 1 \tag{2}$$

$$Inhibition\ effect\left(\%\right) = \frac{G_{t-s}}{(G_{t-s}+1)} \times 100\% \tag{3}$$

Where R_t is the correction factor, $I_{0\text{-}B}$ is the luminescence intensity of the negative control without bacteria, $I_{t\text{-}B}$ is the luminescence intensity value of the negative control with bacteria at time of exposure t, and $G_{t\text{-}s}$ is the Gamma factor for the positive control and the investigated samples, considering their luminescence intensities at the time of exposure t.

2.6. Analytical methods

The concentration of CHA during the photocatalytic experiments was monitored by an ultra-high-performance liquid chromatography (UHPLC; Acquity H Class, Waters) coupled to a single quadrupole mass spectrometry (SQ Detector 2; Waters). Since the concentration of the NAs in the mixture was in a lower range, the concentration of each NA was measured by ultra-high-performance liquid chromatography (UHPLC; Agilent 1290 Infinity II) coupled to a triple quadrupole mass spectrometer (QQQMS; Agilent 6495). Further details of both analysis methods can be found in the Supplementary Information (see Text S1 and Tables S1 and S2).

3. Results and discussion

3.1. Characterization of BC/ZnO

3.1.1. SEM and EDX analyses

SEM and EDX analyses were performed to evaluate the morphology and the elemental composition of the BC/ZnO composite. Fig. 1 shows the SEM images and also EDX results of the synthesized BC/30%ZnO composite. It can be seen in Fig. 1 (a), a porous structure and roughened

Table 1
NAs models investigated in this study.

Chemical structure	Abbreviation	Name	Formula	M.W. (g/mol)	pKa
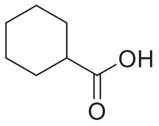	CHA	Cyclohexanecarboxylic acid	$C_7H_{12}O_2$	128.17	4.82*
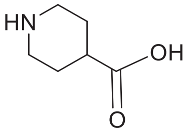	IA	Isonipecotic acid	$C_6H_{11}NO_2$	129.16	pKa$_1$: 3.73; pKa$_2$:10.72
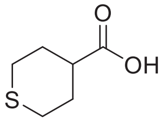	T-2 H-T4CA	Tetrahydro-2 H-thiopyran-4-carboxylic acid	$C_6H_{10}O_2S$	146.21	3.5
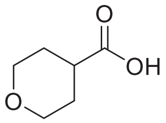	T4CA	Tetrahydropyran-4-carboxylic acid	$C_6H_{10}O_3$	130.14	4.43*
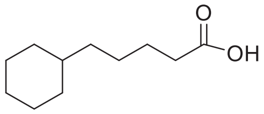	CHPA	Cyclohexanepentanoic acid	$C_{11}H_{20}O_2$	184.27	4.8*
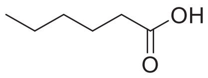	HA	n-caproic acid/ Hexanoic acid	$C_6H_{12}O_2$	116.16	4.88
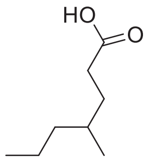	4-MHA	4-methylheptanoic acid	$C_8H_{16}O_2$	144.21	5.23*
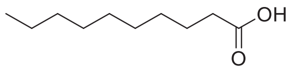	DA	Decanoic acid	$C_{10}H_{20}O_2$	172.26	4.79*

* Values predicted.

surface of the biochar material. Additionally, Fig. 1 (b) to d showcased that the ZnO particles are irregular spherical shapes, and most of them were in the form of aggregates on the biochar. The inhomogeneous structural properties of biochar prove its ability to be a good platform for the ZnO particles to disperse and attach. The presence of Zn was also confirmed from the EDX mapping results shown in Fig. 1 (i). In addition, other elements were detected, such as K and Ca, which should be considered plant ingredients. Similar results were reported for other biomass-based BC/ZnO composites. For instance, Kamal et al. [41] observed the existence of C, O, Ca, Si, K, Mg, Na, P, and Zn elements for the maize straw-based BC/ZnO composite. Pang et al. [35] also reported the presence of K in their coconut shells-derived BC/ZnO composite.

3.1.2. XRD and XPS analyses

Fig. S3 shows the XRD pattern of the Syn-ZnO and the BC/ZnO composite. According to the PDF pattern 04–003-2106 (Zincite, ZnO), the XRD peaks of the Syn-ZnO and BC/ZnO composite were well matched with the characteristic peaks of the hexagonal ZnO system, where the angles of strong and sharp peaks were 31.78°, 34.44°, 36.27°, 47.54°, 56.61°, 62.89°, 66.41°, 67.99°, 69.13°, and 72.59°, indicating good crystallinity and purity, and the biochar did not influence the structure of the ZnO particles [24,42,43]. Besides, the broad peaks at 11.33, 18.14, and 22.64 were recognized as the amorphous phase in the composite, which were attributed to the carbon structure of biochar. These results confirmed the successful synthesis of Syn-ZnO and the BC/ZnO composite.

Figs. S4 and 2 show the XPS spectra of the Syn-ZnO and the BC/30% ZnO composite, respectively. For the Syn-ZnO sample, the survey scan confirmed the presence of oxygen (O 1 s) and Zn as major components (Fig. S4 a). As shown in Fig. S4 (b), the binding energy of O 1 s is resolved into two peaks, where the one at 528.3 eV could be assigned to chemisorbed oxygen species (O_2^-) in the Zn–O bonding of the ZnO wurtzite structure and the other at 530.8 eV could be associated with oxygen-deficient regions ($O^-$and O^{2-} ions) in the sample matrix [44,45]. Besides, the Zn 2p spectra shown in Fig. S4 (c) shows the Zn 2p$_{3/2}$ and Zn 2p$_{1/2}$ peaks at 1018.9 eV and 1042.0 eV, respectively. The binding energy separation between the two peaks is 23.1 eV, which also matched the reference value of ZnO wurtzite. Compared to Syn-ZnO, the survey scan results of the BC/ZnO composite shown in Fig. 2 (a) revealed the existence of carbon (C 1 s) in addition to oxygen (O 1 s) and Zn as major constituents. Furthermore, high-resolution spectra of C 1 s, O 1 s, and Zn 2p were performed to obtain more information. Fig. 2 (b) showed the C 1 s spectra and the three prominent peaks at 284.8 eV, 286.2 eV, and 287.4 eV were attributed to C-C/C = C, C-O, and C = O, respectively [25,46]. According to Fig. 2 (c), the O 1 s peak could be decomposed into two peaks at 531.4 eV and 532.7 eV. The peak with a lower binding energy phase corresponded to the oxygen lattice (O_L), which could be attributed to the Zn-O bond in the ZnO networks. The 532.7 eV peak indicated the oxygen vacancies (O_V) on the surface of the BC/ZnO composite, usually related to surface hydroxyl groups (–OH) [47,48].

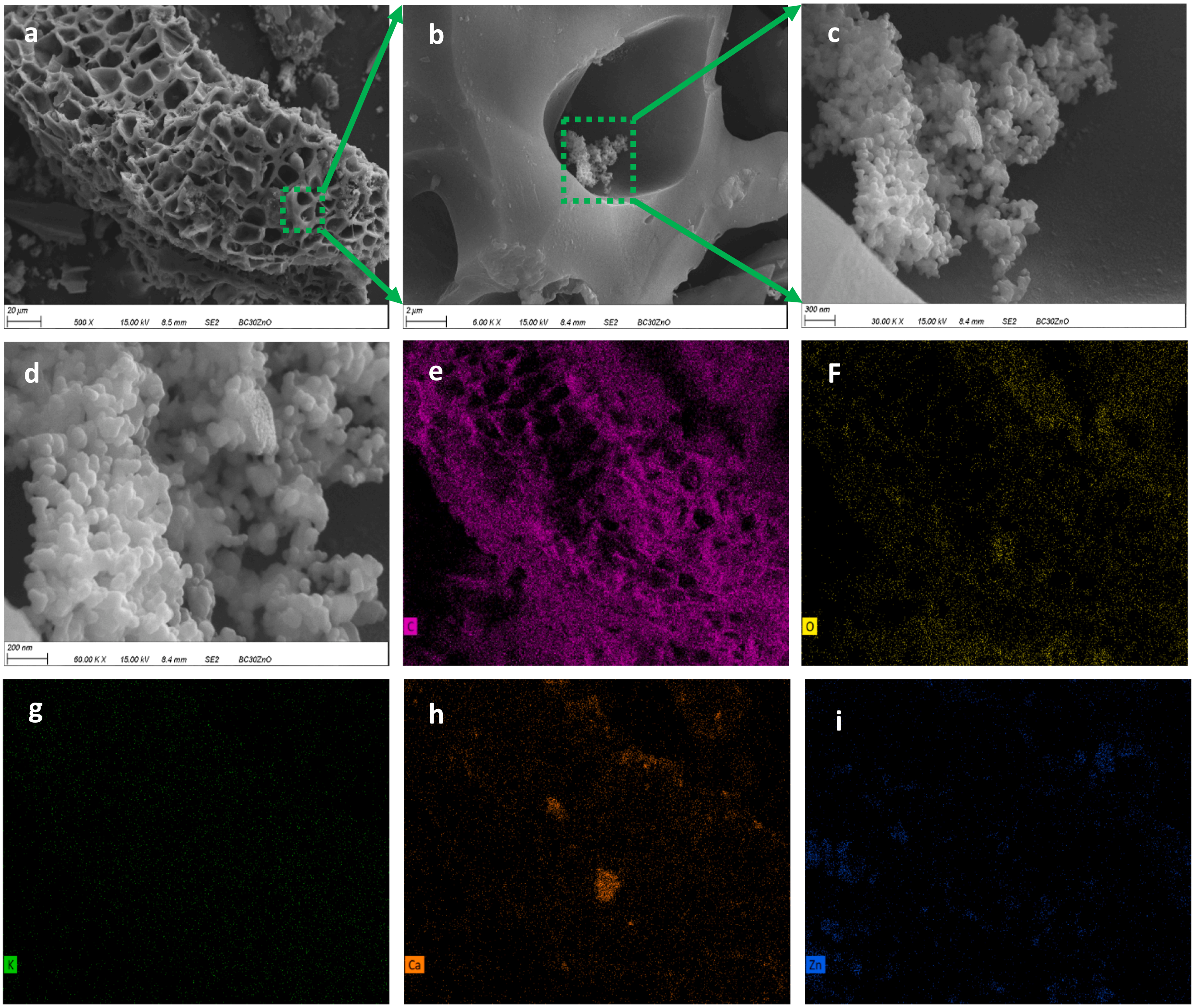

Fig. 1. SEM-EDX results of the BC/30%ZnO composite.

Moreover, the O_V can serve as active sites that trigger the adsorption of O_2 on the surface of the composite, while the adsorbed or chemisorbed O_2, H_2O, or C-O-Zn bond could cause the peak at 532.7 eV [49,50]. In addition, two symmetric peaks were detected at 1022.7 eV and 1045.8 eV in the Zn 2p spectra shown in Fig. 2 (d), which were associated with the Zn $2p_{3/2}$ and Zn $2p_{1/2}$, respectively. The binding energy separation between the two peaks is 23.1 eV, which confirmed the presence of the normal Zn^{2+} valence state in the synthesized BC/ZnO composite by showing highly coincident with the reference value of ZnO wurtzite (~23.0 eV) [25,29,48]. Therefore, all the results from the XPS analysis confirmed the formation of ZnO on the surface of the hard wood-based biochar.

3.1.3. *Optical properties*

Photoluminescence spectroscopy (PL) was employed to study the optical properties of the BC/30%ZnO composite. The PL spectrum could provides useful information regarding the charge carriers transfer at interfaces and photogenerated e^{-}-h^{+} efficiency, which is related to the photocatalytic performance of the photocatalyst [42]. A decrease in PL intensity indicates a lower recombination rate of photogenerated e^{-}-h^{+} [51]. Fig. 3 (a) shows the PL spectra of the BC/30%ZnO composite and Syn-ZnO. It can be seen that the composite showed lower fluorescence intensity compared to Syn-ZnO, which means that the biochar inhibited the recombination of photoinduced e^{-}-h^{+} pairs from ZnO and improved the photocatalytic performance.

Moreover, Fig. 3 (b) shows the UV–vis DRA reflectance spectra of the BC/30%ZnO composite and Syn-ZnO. From the spectra, both the composite and Syn-ZnO showed a characteristic peak at the wavelength of 372 nm. The band gap is the distance between the valence band and the lowest empty conduction band, which could determine the amount of photon energy needed to be absorbed by the semiconductor to cause photo-generation of e^{-}-h^{+} [52]. Based on the Tauc method, the band gap of the composite and Syn-ZnO was calculated from the UV–vis DRA reflectance spectra. The Tauc method has the assumption that the energy-dependent absorption coefficient α can be expressed by Eq. (4), where h is the Plank constant, ν is the photon's frequency, E_g is the band gap energy, and B is a constant. Furthermore, combined with the Kubelka-Munk function (Eq. (5), the Tauc equation could be transformed into Eq. (6), where R_∞ is the reflectance obtained from the UV–vis reflectance spectra, and K and S are the absorption and scattering coefficients, respectively. According to Eq. (5), the absorbance response could be calculated from the reflectance, and the results are presented in

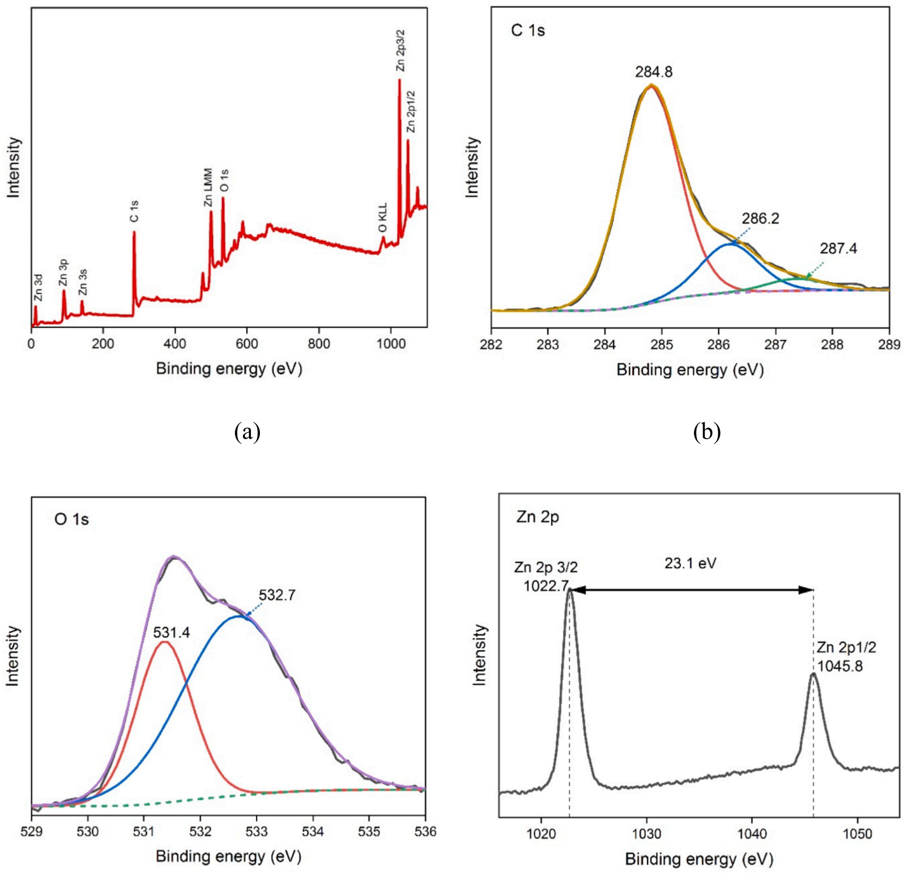

(a) (b)

(c) (d)

Fig. 2. (a) XPS survey scan spectrum of the BC/30%ZnO and high-resolution XPS spectra of (b) C 1 s (c) O 1 s, and (d) Zn 2p.

Fig. 3 (c). It is obvious that both BC/30%ZnO composite and Syn-ZnO had strong responses below 400 nm, which mainly assigned to the intrinsic band absorption of ZnO as a semiconductor [47]. In addition, the composite showed stronger responses to visible light than Syn-ZnO. Yang et al. [24] reported similar UV–vis DRS results, where the ZnO@C composite showed a stronger response to visible light than synthesized ZnO.

In general, the γ factor in Eq. (6) is equal to 1/2 or 2 for the direct and indirect transition band gaps, respectively [53]. As shown in Fig. 3 (d) and (e), using the Tauc method, the band gap of BC/30%ZnO and Syn-ZnO were determined as 3.21 eV and 3.26 eV, respectively. Several studies have observed similar results in the slightly decreased band gap of the BC/ZnO composite compared to pure ZnO. This could be explained by the electronic interaction between carbon and metal oxide, which could absorb more photons and be utilized in photocatalytic reactions, resulting in a higher photocatalytic activity than pure ZnO [24,25]. Furthermore, Mankomal and Kaur [50] explained that the narrowed band gap of the composite is possibly caused by the formation of the Zn-O-C bond, which allowed the electrons to transfer from ZnO to the surface of the biochar.

$$(\alpha \bullet h\nu)^{1/\gamma} = B(h\nu - E_g) \tag{4}$$

$$F(R_\infty) = \frac{K}{S} = \frac{(1-R_\infty)^2}{2R_\infty} \tag{5}$$

$$(F(R_\infty) \bullet h\nu)^{1/\gamma} = B(h\nu - E_g) \tag{6}$$

3.2. Effects of ZnO content and catalyst dosage on CHA degradation

As a cyclic aliphatic carboxylic acid, CHA is one of the typical classical NAs used to study the degradation of model NAs [12,54]. In this study, CHA was selected to evaluate the photocatalytic performance of BC/ZnO composites under simulated solar light. 25 mg/L CHA was prepared with carbonate buffer to keep the pH stable around 8.5. Before the photocatalytic experiments, control experiments were conducted at dark conditions using BC, Syn-ZnO, and BC/30%ZnO to evaluate the adsorption capacity of the individual materials and the prepared composite. Experiments using only CHA under simulated solar irradiation were also performed (photolysis control). Fig. S5 (a-c) showed that no removal of CHA was found by adsorption under dark conditions in 120 min. In addition, Fig. S5 (d) indicates that in the absence of the composite, simulated solar light did not result in any CHA removal, even after 360 min of irradiation time.

To understand the effect of ZnO content on the photocatalytic performance of the composite, different composites with 10, 20, 30, and 50 wt% of ZnO were designed and synthesized. Fig. 4 (a) describes the photocatalytic degradation profile of CHA using different BC/ZnO composites with the same dosage (0.5 mg/L). According to Fig. 4 (b), in 4 h of simulated solar irradiation, the total degradation efficiency of CHA was 61.2 % and 85.4 % using BC/10%ZnO and BC/20%ZnO, respectively. However, a 93.7 % CHA degradation efficiency was found when the composite with 30 wt% ZnO was tested. With increasing the ZnO content to 50 wt%, there was a slight decreasing effect on the degradation of CHA. He et al. [49] also observed similar results in the photocatalytic degradation of methylene blue by BC/ZnO under UV–visible light, reporting a moderate decrease in the degradation

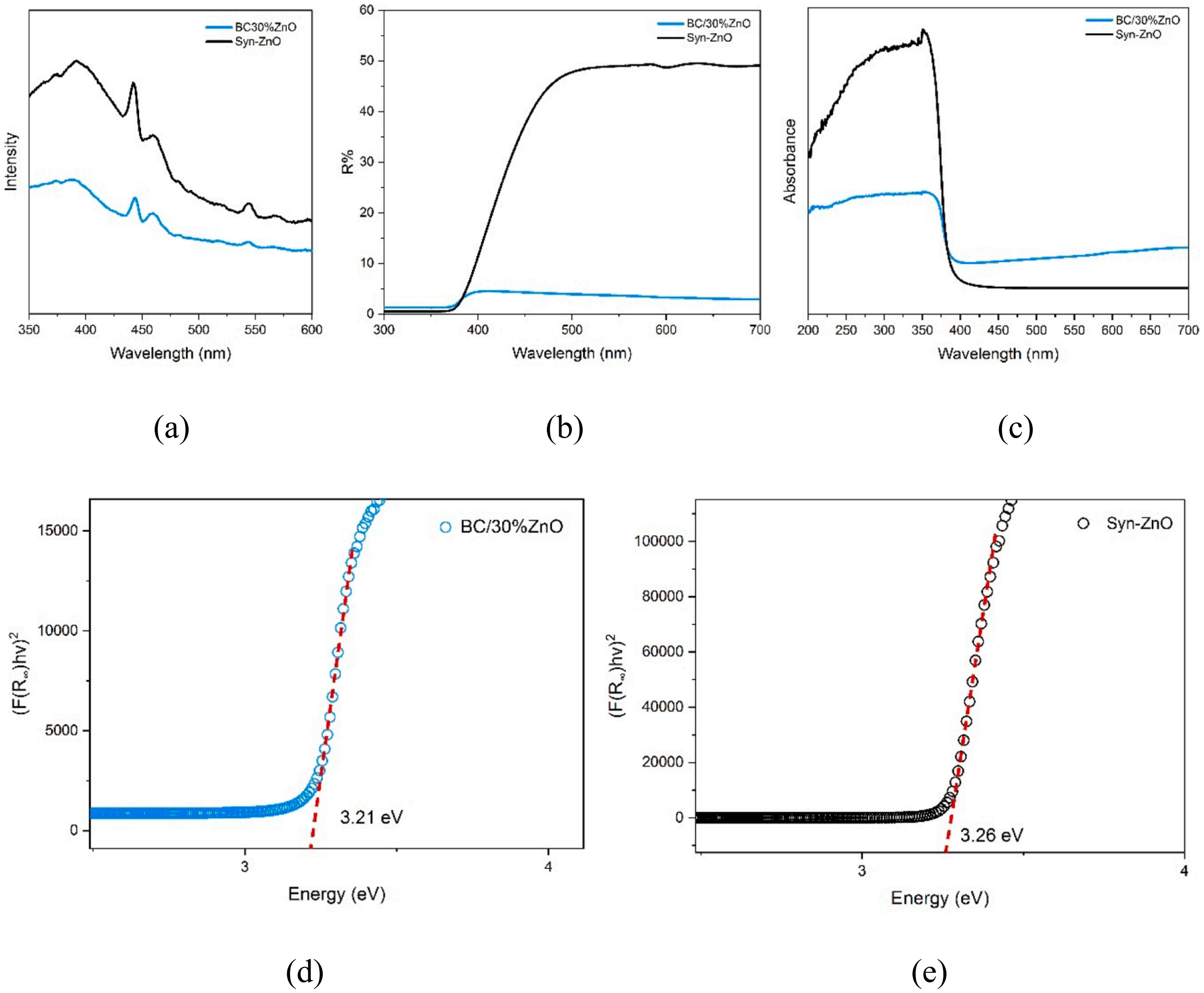

(a) (b) (c)

(d) (e)

Fig. 3. (a) PL spectrum, (b) UV–vis DRA reflectance, and (c) absorbance response plot spectrum of the BC/30%ZnO composite and Syn-ZnO. Tauc plot of (d) BC/30% ZnO composite and (e) Syn-ZnO were obtained with diffusion reflectance spectroscopy.

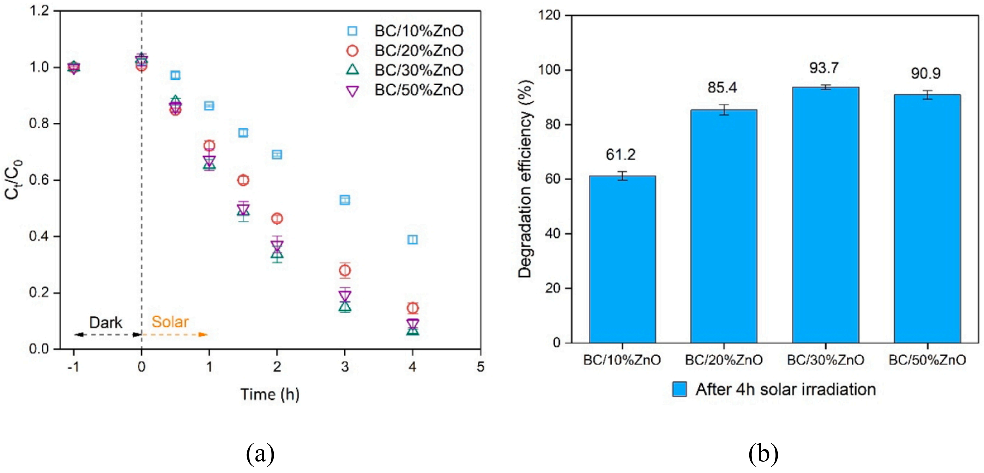

(a) (b)

Fig. 4. CHA degradation using different BC/ZnO composites under simulated solar irradiation: (a) C_t/C_0 vs. Time; (b) Degradation efficiencies using composites with different content of ZnO.

efficiency (98.7 % to 83.0 %) while increasing the BC/ZnO molar ratio from 1:0.5 to 1:2. This is probably associated with the higher generation of radical species, which can result in a faster rate of recombination reactions and a decrease in the performance of the degradation process. Based on the results described above, the BC/30%ZnO composite was selected as the best material for the following experiments in this study.

Fig. 5 shows the effect of different BC/30%ZnO dosages (0.1, 0.25, 0.5, 1.0, and 2.0 g/L) and simulated solar irradiation times on CHA

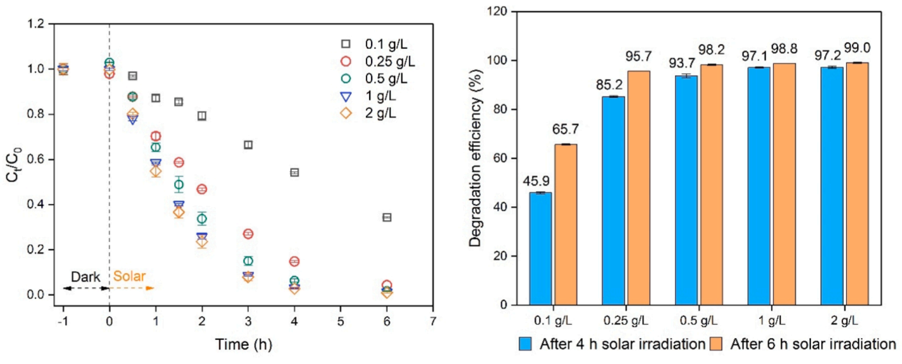

(a) (b)

Fig. 5. CHA degradation using different dosages of BC/30%ZnO under simulated solar irradiation: (a) C_t/C_0 vs. Time; (b) Comparison at different simulated solar irradiation times.

degradation. The degradation of CHA by BC/30%ZnO followed a pseudo-first order (PFO) kinetics model, and the rate constants were summarized in Table 2. The degradation efficiency of CHA showed a rapid increase in the kinetic constants (k_{PFO}) from 0.179 to 0.132 h^{-1} when the composite dose increased from 0.1 g/L to 0.5 g/L. Then, the increase slowed down with the composite dosage from 0.5 g/L to 2 g/L. While increasing the concentration of the composite, more photocatalytic active sites are available to absorb photons and generate more reactive species that could quickly degrade the target contaminant [12]. However, increasing the composite dosage above the optimum concentration could lead to the occurrence of the scattering effect and a reduction in simulated solar light penetration depth, resulting in less increase in the degradation efficiency of CHA [28,55]. Moreover, Fig. 5 (b) shows no significant differences in the degradation percentage, increasing the irradiation time from 4 to 6 h. Considering the cost and effectiveness, the best experimental conditions for the following experiments were 0.5 g/L BC/30%ZnO and 4 h of simulated solar irradiation. To demonstrate the better photocatalytic performance of the prepared BC/30%ZnO composite, Syn-ZnO was applied using the same amount of ZnO present in 0.5 g/L BC/30%ZnO composite, resulting in a degradation efficiency of 48.3 % in 6 h of treatment (see Fig. S6). Therefore, the photocatalytic performance of the BC/30%ZnO composite has been enhanced to approximately two-fold that the pure Syn-ZnO.

3.3. *ROS and possible mechanism of BC/ZnO under simulated solar irradiation*

EPR analysis was conducted with different probe chemicals to identify the main ROS involved in the degradation mechanism of CHA. DMPO and BMPO were used to identify $^\bullet$OH and $O_2^{\bullet-}$ species, respectively. As shown in the EPR spectra (Fig. 6 a), no signal of DMPO-derived adduct was detected using the composite at dark conditions. However, after 5 min under simulated solar light, the peaks of the adduct DMPO-$^\bullet$OH were identified for both the BC/30%ZnO composite and Syn-ZnO, showing typical pattern signals with an approximate intensity ratio of 1:2:2:1 [56,57]. Although the results confirmed that the BC/30% ZnO composite and *syn*-ZnO generated $^\bullet$OH, the DMPO-$^\bullet$OH peaks were much more intense using the BC/30%ZnO system. This may suggest that loading ZnO on the BC surface results in a higher generation of $^\bullet$OH species during the CHA photodegradation process, i.e., better photocatalytic properties.

Table 2
PFO kinetics parameters of the BC/30%ZnO composite at different dosages.

Dosage of BC/30%ZnO (g/L)	k_{PFO} (h^{-1})	R^2
0.1	0.179	0.980
0.25	0.530	0.988
0.5	0.732	0.997
1	0.807	0.980
2	0.830	0.985

The formation of $O_2^{\bullet-}$ species was also investigated by EPR measurements using BMPO as trapping agent. EPR spectra was collected in 2.5 min of simulated solar irradiation using the composite. The appearance of strong peaks for BMPO-$^\bullet$OH spin adducts is shown in Fig. 6 (b), which complements the results obtained with DMPO. Additionally, the formation of four low-intensity peaks next to the BMPO-•OH peaks was also found. Antonopoulou et al. [58] obtained similar peaks by EPR spectra with BMPO, and the four tiny peaks could be attributed to the BMPO adducts with $O_2^{\bullet-}$. In this sense, the observed signals prove the simultaneous generation of both $^\bullet$OH and $O_2^{\bullet-}$ species. In addition, TEMP was applied as another probe chemical to identify the presence of $^1O_2$. According to the EPR spectra shown in Fig. 6 (c), no signals of $^1O_2$ were detected. Considering all the observations from EPR spectra, it appears that $^\bullet$OH species play an important role in the degradation mechanism of CHA, while $O_2^{\bullet-}$ may have a low contribution.

Combined with the results from EPR analysis and the characteristics of the composite, the degradation mechanism of the BC/30%ZnO composite under simulated solar light is illustrated in Fig. 7, which is similar to the results reported by other published studies [49,50,59,60]. With narrow band gaps, by acquiring photon energy from simulated solar radiation, the photogenerated e^- transferred from the gap band phase to the conduction phase while h^+ were generated on the surface of BC/30%ZnO composite, and the biochar inhibited the recombination of the e^--h^+ pairs (Eqs. (7) to (9). The production of $^\bullet$OH species could be mainly attributed to the reaction of the generated h^+ with water molecules and hydroxyl groups (Eqs. (10) and (11). Besides, e^--h^+ could react with oxygen and generate $O_2^{\bullet-}$, which could directly attend to the degradation process of CHA. On the other hand, $O_2^{\bullet-}$ could also convert to $^\bullet$OH by reactions shown in Eqs. (12) to (15). With $^\bullet$OH playing the dominant role, the CHA is eventually degraded with high efficiency using the BC/30%ZnO composite under simulated solar light.

$$ZnO(e^-) + BC \rightarrow BC(e^-) + ZnO \tag{7}$$

$$BC/30\%ZnO + h\nu \rightarrow BC/30\%ZnO(h^+ + e^-) \tag{8}$$

$$2ZnO + h\nu \rightarrow ZnO(h^+) + ZnO(e^-) \tag{9}$$

$$ZnO(h^+) + H_2O \rightarrow ZnO + {}^\bullet OH \tag{10}$$

$$ZnO(h^+) + OH^- \rightarrow ZnO\ +\ {}^\bullet OH\ +\ H^+ \tag{11}$$

$$BC(e^-) + O_2 \rightarrow BC + O_2^{\bullet-} \tag{12}$$

$$O_2^{\bullet-}\ +\ H_2O \rightarrow {}^\bullet HO_2 + OH^- \tag{13}$$

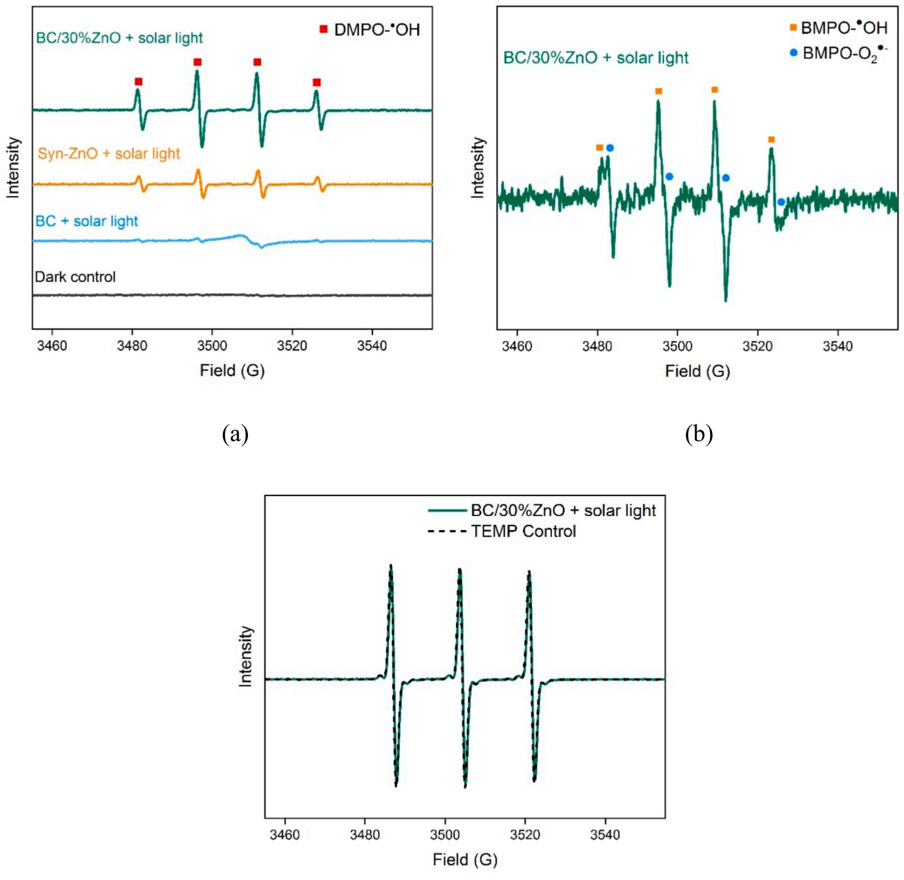

(a)

(b)

(c)

Fig. 6. EPR spectra using (a) DMPO, (b) BMPO, and (c) TEMP as trapping agents.

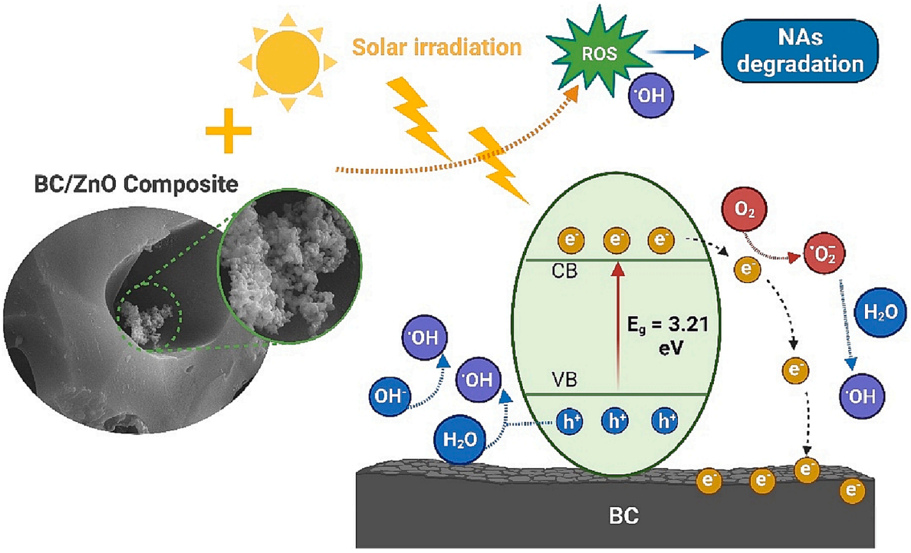

Fig. 7. Schematic representation of photocatalytic mechanism for the degradation of NAs using the BC/30%ZnO composite under simulated solar irradiation.

$$^{\bullet}HO_2 + {}^{\bullet}HO_2 \rightarrow H_2O_2 + O_2 \tag{14}$$

$$H_2O_2 + BC(e^-) + ZnO(e^-) \rightarrow BC/ZnO + \bullet OH \tag{15}$$

3.4. Reusability of BC/30%ZnO composite

The reusability and stability of photocatalysts are critical considerations that could affect the practical application of these materials. Therefore, the photocatalytic performance of the BC/30%ZnO composite was investigated through successive cycles of use. The degradation efficiency was calculated after each cycle and shown in the bar chart in Fig. 8. After 4 cycles of use, the efficiency of the composite for CHA degradation was still up to 92.9 %, which clearly indicated that the composite showed good stability and reusability. In addition, after 4 times use, SEM images of the BC/30%ZnO composite were captured to identify possible changes in the morphology of the material. Comparing the SEM images of the composite before and after use (see Fig. S7), no significant differences were observed for the porous structure biochar platform and the attached ZnO particles. Some studies have reported similar reusability results, however, applying shorter treatment times. For instance, Chen et al. [29] developed a BC/ZnO composite from jute fibers for the photodegradation of methylene blue dye, achieving almost 100 % degradation efficiency in the 1st cycle under 1 h UV irradiation, and over 80 % for the 7th run. Jahani et al. [61] applied a milkvetch-derived BC/Zn-Ce oxide nanocomposite for the decontamination of reactive blue 19 containing solutions, decreasing the degradation efficiency by roughly 6 % in the 5th compared to the 1st cycle (under LED irradiation for 1 h with 1 mL of H_2O_2). Therefore, the BC/30%ZnO composite proposed in our study performed high photocatalytic degradation while maintaining notable chemical and physical stability over repeated cycles.

3.5. *Degradation performance towards NAs mixture*

To further evaluate the photocatalytic performance of the BC/30% ZnO composite, a complex mixture containing eight different NAs (5 mg/L each) was used as the target contaminated solution. Considering the increased initial total concentration of the target contaminant (40 mg/L), the simulated solar irradiation time was increased to 6 h accordingly, with 0.5 g/L of BC/30%ZnO composite results obtained for the CHA. Before the simulated solar irradiation started, the photodegradation and dark adsorption control were conducted for the mixture solution. No degradation of all NAs was found without the presence of composite at dark conditions (Fig. S8), which confirmed the degradation of the target NAs was due to the simultaneous presence of the composite and the simulated solar light.

To complement this result, the determination of the point of zero charge (PZC) of the material was carried out using the salt addition method [36,37]. In addition, the experimental and predicted pKa values for all NAs were also provided in Table 1. From our observation, the PZC of the material was found to be 7.74 (see Fig. S9), which is lower than the pH of the mixture (8.50). In this case, it is possible to assume that the surface of BC/30%ZnO is negatively charged in solution. As the pKa of all NAs is also lower than the pH of the matrix (see values in Table 1), the NAs are primarily in their anionic form, and the interaction between them and the material is predominantly repulsive, explaining the negligible degree of adsorption described above. In this sense, it is reasonable to assume that the differences in the degradation kinetics of some NAs are mainly associated with the distinct functional groups in their structure that can provide different levels of reactivity to $^{\bullet}$OH species, which, despite non-selective, have specific kinetic reactions depending on the nature of the organic molecule.

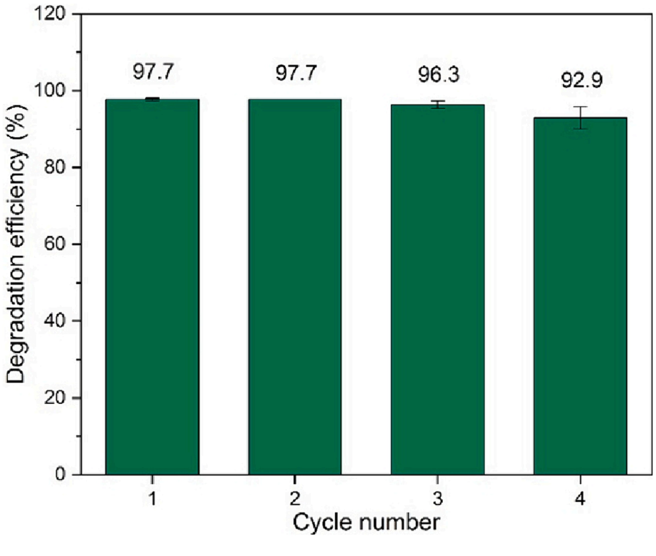

Fig. 8. Reusability tests for the BC/30%ZnO composite.

Considering this, the degradation process of each NAs in the mixture is represented in Fig. 9 (a-b). All NAs achieved an efficient degradation rate by the composite under simulated solar irradiation, while different degradation efficiencies were observed. For example, the T-2H-T4CA was fully degraded by BC/30%ZnO composite in 2 h, but only after 4 h of irradiation most of the NAs in the mixture reached nearly 100 % degradation, including CHA (99.7 %), CHPA (>99 %), HA (98.8 %), 4-MHA (99.68 %), and DA (>99 %). In contrast, the degradation percentage of IA and T4CA was lower than that of other NAs after 4 h of irradiation; however, within 6 h of treatment, they reached a final degradation of over 80 %. Consequently, the total degradation efficiency of the 8 NAs in the mixture reached 95.5 % using the composite under 6 h of simulated solar light.

The degradation process of the different NAs all fitted with PFO kinetics, and the corresponding degradation rates are shown in Fig. 9 (c). T-2H-T4CA had the fastest degradation rate (2.90 h^{-1}) among all NAs, which was 2.90 times the reaction rate of CHA in the mixture. This could be due to the structure of T-2H-T4CA, where the non-bonding electrons of S atoms could enhance its overall reactivity towards oxidizing species. de Oliveira Livera et al. [62] investigated the structure–reactivity relationship of NAs in the photocatalytic degradation process using 0.5 g/L TiO_2 as photocatalyst under UV irradiation and it was reported that the degradation rate for T-2H-T4CA was 2.67 times of that for CHA.

In the mixture, the degradation rate for the eight model NAs follows the order: T-2H-T4CA > CHPA > CHA > 4-MHA > DA > HA > T4CA > IA. According to these results, the NAs with saturated rings such as CHPA and CHA showed higher reaction rates than the linear chain structured NAs (4-MHA, DA, and HA), indicating that the single saturated ring could increase the reactivity of the compound. A similar tendency was also proved by de Oliveira Livera et al. [62], where the degradation rate of 4-pentylcyclohexanoic acid (4pnCHA) was 1.38 times the rate of linear dodecanoic acid (DDA). Besides, Afzal et al. [63] found that compared to small, linear, and acyclic NAs, reactivity favored large, branched, and cyclic NAs, leading to a better oxidization performance by the UV/H_2O_2 process, in which $^{\bullet}$OH also have the main role in the degradation mechanism. The preferential degradation observed in our study also supported this finding. Compared to CHA, CHPA has a longer branch attached to the saturated ring and showed a faster degradation rate. In addition, among the linear chain structured NAs in the mixture, DA has a carbon number of 10, and the reaction rate was 1.18 times the rate of HA, which has a carbon number of 6. Furthermore, 4-MHA showcased a faster reaction rate with less carbon number compared to DA, which could be attributed to the introduction of the tertiary carbon by the alkyl branching-point. The tertiary carbon-centered radicals have higher stability than primary and secondary radicals, which could increase the oxidation rate [63]. Moreover, Meng et al. [12] evaluated the photocatalytic activity of Bi_2WO_6 (1 g/L) with simulated solar light by applying 4 different NAs (individually) as the target pollutants, and the degradation rates were reported in the following order: T-2H-T4CA > CHA > IA > T4CA. Compared to that work, in our study, the BC/30%ZnO composite showed better photocatalytic degradation performance for the IA and T4CA degradation, even using a more complex matrix.

Moreover, the acute toxicity of NAs in both the untreated matrix and the treated solution using BC/30%ZnO under 6 h of simulated solar irradiation was assessed based on the inhibition of bioluminescence in *V. fischeri* bacteria. As shown in Fig. S10, the *V. fischeri* inhibition decreased

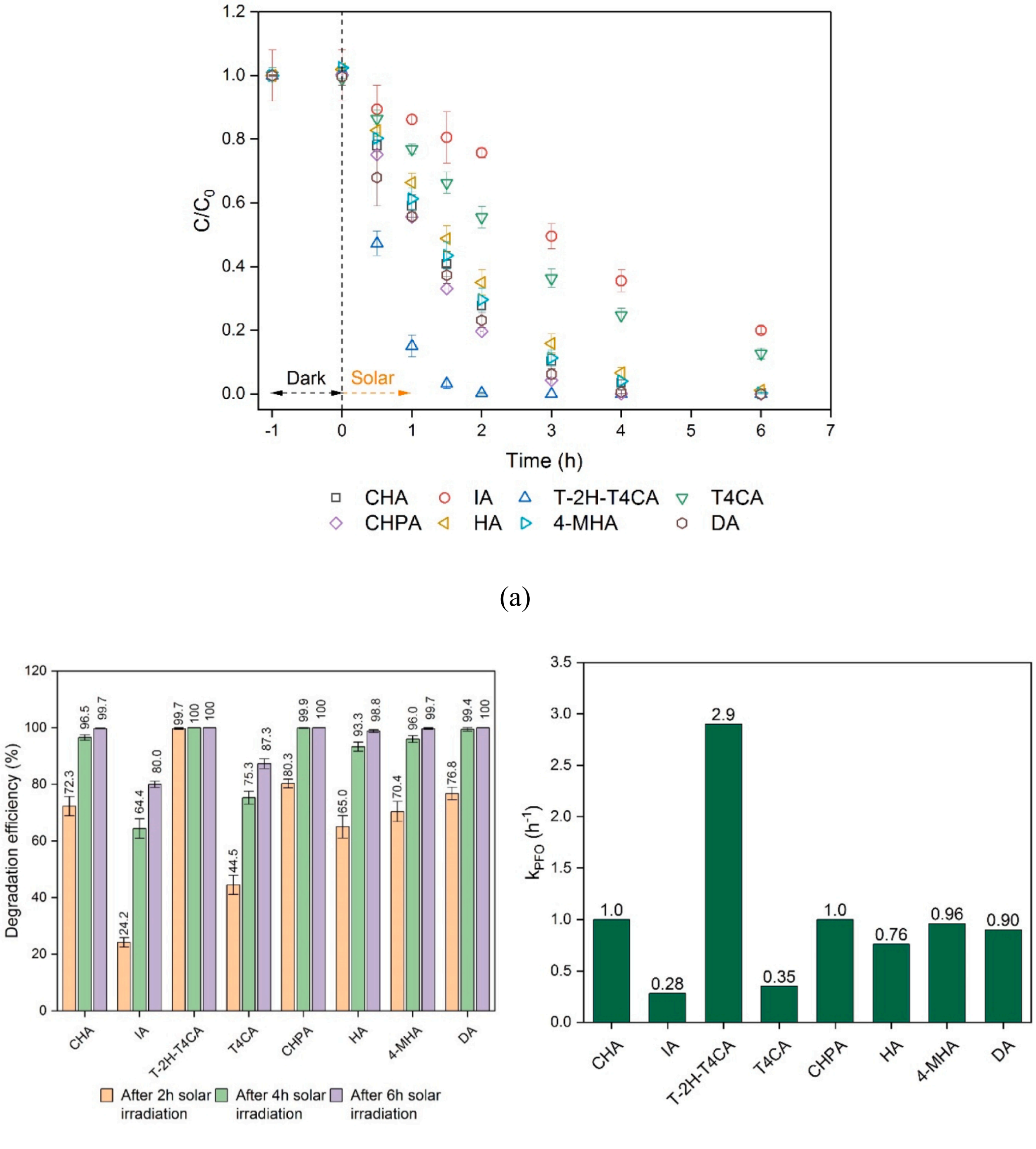

(a)

(b)

(c)

Fig. 9. Simultaneous degradation of a mixture of eight NAs using the BC/30%ZnO composite under simulated solar irradiation.

from 68.2 % to 41.4 % after 5 min of exposure to the treated matrix, and from 66.5 % to 44.0 % after 15 min, i.e., attaining a reduction of over 39.3 % and 33.8 %, respectively. This reduction in the acute toxicity of the NAs in the mixture after 6 h of treatment using the BC/30%ZnO composite suggests that the by-products formed during the degradation process of the NAs are, at least in general, less toxic than the parent compounds.

3.6. *Leaching test*

A leaching test was conducted to investigate the potential release of Zn from the composite material into the solution. For that, 0.5 g/L of the BC/30%ZnO composite were dispersed into 60 mL of buffer solution (5 mM $NaHCO_3$) and mixed continuously for 24 h under dark conditions. Then, samples were collected, filtered by a 0.2 μm filter, and analyzed by ICP-OES. After 24 h of mixing, a low concentration of Zn of 38 μg/L was measured in the sample, meaning that approximately 0.05 % of the total content of Zn in the composite was released into the solution. This confirms the good stability of the composite material, even after 24 h of contact with the solution. Jusoh et al. [64] developed mesostructured silica nanoparticles loaded with ZnO (ZnO/MSN) as photocatalyst, and they reported 2.97 % (equivalent to 148.5 μg/L) of Zn leaching after 8 h UV irradiation using 1 g/L of ZnO/MSN. The United States Environmental Protection Agency (US EPA) published an acute and chronic criterion of 120 μg/L as the limit of Zn for the protection of freshwater aquatic life [65]. Therefore, the measured leached Zn concentration in our study is lower than the recommended limit, suggesting the environmental compatibility of the proposed treatment.

4. Conclusions and future perspectives

This work successfully incorporated ZnO particles into a porous and roughened platform derived from a sustainable BC source. BC played an important role as an electron reservoir that could reduce the recombination rate of photogenerated e^{-}-h^{+} in the BC/30%ZnO composite. Based on the degradation of CHA, the best experimental conditions were determined as 0.5 g/L BC/30%ZnO and 4 h of simulated solar irradiation time, achieving 93.7 % degradation efficiency following a PFO kinetic. $^{\bullet}$OH species detected by EPR measurements were found to have an important role in CHA degradation, and the composite showed good reusability and stability after 4 successive cycles of use. The BC/30% ZnO compound was also successfully tested, for the first time, for the simultaneous degradation of a complex mixture of eight NAs with significantly different structures, achieving a total degradation efficiency of more than 95.5 % in 6 h of simulated solar irradiation, while decreasing the acute toxicity of the solution by about 45 % towards *V. fischeri*. The degradation rate following the order T-2H-T4CA > CHPA > CHA > 4-MHA > DA > HA > T4CA > IA.

Considering the excellent photocatalytic performance of the BC/30% ZnO composite for NAs degradation, as well as its good reusability and stability, this photocatalyst is a sustainable approach for the treatment of real OSPW. In future studies, exploring the effect of different synthesis temperatures on the photocatalytic reactivity of BC/ZnO composites toward degrading NAs would be valuable. Additionally, in scale-up applications, reducing the catalyst dosage and utilizing solar natural light as the irradiation source could be considered. Moreover, integrating BC/ZnO composites with solar light into established OSPW treatment methods, such as wetlands, holds promise. By combining wood waste-based biochar with low ZnO content, solar radiation as a green energy source, and employing low composite dosage, this research offers an eco-friendly and cost-effective approach to removing NAs from water.

CRediT authorship contribution statement

Zhexuan An: Writing – review & editing, Writing – original draft, Visualization, Methodology, Investigation, Formal analysis, Data curation. **Isaac Sánchez-Montes:** Writing – review & editing, Supervision. **Pamela Chelme-Ayala:** Writing – review & editing, Supervision. **Chunmao Chen:** Writing – review & editing. **Mohamed Gamal El-Din:** Writing – review & editing, Supervision, Resources.

Declaration of competing interest

The authors declare that they have no known competing financial interests or personal relationships that could have appeared to influence the work reported in this paper.

Data availability

Data will be made available on request.

Acknowledgments

This work was supported by the Natural Sciences and Engineering Research Council of Canada (NSERC) Senior Industrial Research Chair (IRC) in Oil Sands Tailings Water Treatment, and Canada's Oil Sands Innovation Alliance (COSIA), Syncrude Canada Ltd., Suncor Energy Inc., Canadian Natural Resources Ltd., Imperial Oil Resources, Teck Resources Limited, EPCOR Water Services, Alberta Innovates, and Alberta Environment and Parks. This research is also supported by the University of Alberta's Future Energy Systems research initiative, supported by the Canada First Research Excellence Fund and an NSERC Discovery Grant. The authors are also grateful to Dr. Muhammad Arslan and Dr. Lingling Yang for their help and support in the toxicity assays and analytical measurements, respectively.

Appendix A. Supplementary data

Supplementary data to this article can be found online at https://doi.org/10.1016/j.cej.2024.151308.

References

[1] P.J. Quinlan, K.C. Tam, Water treatment technologies for the remediation of naphthenic acids in oil sands process-affected water, Chem. Eng. J. 279 (2015) 696–714.

[2] C. Whitby, Chapter 3 - Microbial Naphthenic Acid Degradation, in: Advances in Applied Microbiology, Academic Press, 2010, pp. 93–125.

[3] E.W. Allen, Process water treatment in Canada's oil sands industry: I. Target pollutants and treatment objectives, J. Environ. Eng. Sci. 7 (2) (2008) 123–138.

[4] D. Jones, C.E. West, A.G. Scarlett, R.A. Frank, S.J. Rowland, Isolation and estimation of the 'aromatic' naphthenic acid content of an oil sands process-affected water extract, J. Chromatogr. A 1247 (2012) 171–175.

[5] J. Masliyah, Z.J. Zhou, Z. Xu, J. Czarnecki, H. Hamza, Understanding water-based bitumen extraction from athabasca oil sands, Can. J. Chem. Eng. 82 (4) (2004) 628–654.

[6] J.S. Clemente, P.M. Fedorak, A review of the occurrence, analyses, toxicity, and biodegradation of naphthenic acids, Chemosphere 60 (5) (2005) 585–600.

[7] R.A. Frank, K. Fischer, R. Kavanagh, B.K. Burnison, G. Arsenault, J.V. Headley, K. M. Peru, G.V.D. Kraak, K.R. Solomon, Effect of carboxylic acid content on the acute toxicity of oil sands naphthenic acids, Environ. Sci. Tech. 43 (2) (2009) 266–271.

[8] M.O. Hagen, B.A. Katzenback, M.D.S. Islam, M. Gamal El-Din, M. Belosevic, The analysis of goldfish (Carassius auratus L.) innate immune responses after acute and subchronic exposures to oil sands process-affected water, Toxicol. Sci. 138 (1) (2013) 59–68.

[9] C. Li, L. Fu, J. Stafford, M. Belosevic, M. Gamal El-Din, The toxicity of oil sands process-affected water (OSPW): a critical review, Sci. Total Environ. 601 (2017) 1785–1802.

[10] M.D. MacKinnon, H. Boerger, Description of two treatment methods for detoxifying oil sands tailings pond water, Water Quality Res. J. 21 (4) (1986) 496–512.

[11] R. Huang, Y. Chen, M.N.A. Meshref, P. Chelme-Ayala, S. Dong, M.D. Ibrahim, C. Wang, N. Klamerth, S.A. Hughes, J.V. Headley, K.M. Peru, C. Brown, A. Mahaffey, M. Gamal El-Din, Characterization and determination of naphthenic acids species in oil sands process-affected water and groundwater from oil sands development area of Alberta, Canada, Water Res. 128 (2018) 129–137.

[12] L. Meng, Z.T. How, S.O. Ganiyu, M. Gamal El-Din, Solar photocatalytic treatment of model and real oil sands process water naphthenic acids by bismuth tungstate: Effect of catalyst morphology and cations on the degradation kinetics and pathways, J. Hazard. Mater. 413 (2021) 125396.

[13] M. Hendrikse, D.P. Gaspari, A.D. McQueen, C.M. Kinley, A.J. Calomeni, T.D. Geer, M.C. Simair, K.M. Peru, J.V. Headley, J.H. Rodgers, J.W. Castle, Treatment of oil sands process-affected waters using a pilot-scale hybrid constructed wetland, Ecol. Eng. 115 (2018) 45–57.

[14] Leshuk, T.M.C., Young, Z.W., Wilson, B., Chen, Z.Q., Smith, D.A., Lazaris, G., Gopanchuk, M., McLay, S., Seelemann, C.A., Paradis, T., Bekele, A., Guest, R., Massara, H., White, T., Zubot, W., Letinski, D.J., Redman, A.D., Allen, D.G., and Gu, F. 2024. A Light Touch: Solar Photocatalysis Detoxifies Oil Sands Process-Affected Waters Prior to Significant Treatment of Naphthenic Acids. ACS ES&T Water.

[15] L.A. Pérez-Estrada, X. Han, P. Drzewicz, M. Gamal El-Din, P.M. Fedorak, J. W. Martin, Structure–reactivity of naphthenic acids in the ozonation process, Environ. Sci. Tech. 45 (17) (2011) 7431–7437.

[16] R. Qin, P. Chelme-Ayala, M. Gamal El-Din, The impact of oil sands process water matrix on the ozonation of naphthenic acids: from a model compound to a natural mixture, Can. J. Civ. Eng. 47 (10) (2020) 1166–1174.

[17] M. Arslan, S.O. Ganiyu, D.M.E. Lillico, J.L. Stafford, M. Gamal El-Din, Fate of dissolved organics and generated sulfate ions during biofiltration of oil sands process water pretreated with sulfate radical advanced oxidation process, Chem. Eng. J. 458 (2023) 141390.

[18] C. Wang, N. Klamerth, R. Huang, H. Elnakar, M. Gamal El-Din, Oxidation of oil sands process-affected water by potassium ferrate (VI), Environ. Sci. Tech. 50 (8) (2016) 4238–4247.

[19] Y. Zhang, N. Klamerth, S.A. Messele, P. Chelme-Ayala, M. Gamal El-Din, Kinetics study on the degradation of a model naphthenic acid by ethylenediamine-N, N'-disuccinic acid-modified Fenton process, J. Hazard. Mater. 318 (2016) 371–378.

[20] Z. Fang, R. Huang, Z.T. How, B. Jiang, P. Chelme-Ayala, Q. Shi, C. Xu, M.G. El-Din, Molecular transformation of dissolved organic matter in process water from oil and gas operation during UV/H2O2, UV/chlorine, and UV/persulfate processes, Sci. Total Environ. 730 (2020) 139072.

[21] D. Ma, H. Yi, C. Lai, X. Liu, X. Huo, Z. An, L. Li, Y. Fu, B. Li, M. Zhang, L. Qin, S. Liu, L. Yang, Critical review of advanced oxidation processes in organic wastewater treatment, Chemosphere 275 (2021) 130104.

[22] M. Priyadarshini, I. Das, M.M. Ghangrekar, L. Blaney, Advanced oxidation processes: Performance, advantages, and scale-up of emerging technologies, J. Environ. Manage. 316 (2022) 115295.

[23] X. Xu, L. Meng, Y. Dai, M. Zhang, C. Sun, S. Yang, H. He, S. Wang, H. Li, Bi spheres SPR-coupled Cu2O/Bi2MoO6 with hollow spheres forming Z-scheme Cu2O/Bi/Bi2MoO6 heterostructure for simultaneous photocatalytic decontamination of sulfadiazine and Ni(II), J. Hazard. Mater. 381 (2020) 120953.

[24] C. Yang, X. Wang, Y. Ji, T. Ma, F. Zhang, Y. Wang, M. Ci, D. Chen, A. Jiang, W. Wang, Photocatalytic degradation of methylene blue with ZnO@C nanocomposites: Kinetics, mechanism, and the inhibition effect on monoamine oxidase A and B, NanoImpact 15 (2019) 100174.

[25] H. Cai, D. Zhang, X. Ma, Z. Ma, A novel ZnO/biochar composite catalysts for visible light degradation of metronidazole, Sep. Purif. Technol. 288 (2022) 120633.

[26] K.M. Mohamed, J.J. Benitto, J.J. Vijaya, M. Bououdina, Recent advances in ZnO-based nanostructures for the photocatalytic degradation of hazardous, non-biodegradable medicines, Crystals 13 (2) (2023) 329.

[27] J. Kahkeci, M. Gamal El-Din, Biochar-supported photocatalysts: Performance optimization and applications in emerging contaminant removal from wastewater, Chem. Eng. J. 476 (2023) 146530.

[28] N.P.F. Gonçalves, M.A.O. Lourenço, S.R. Baleuri, S. Bianco, P. Jagdale, P. Calza, Biochar waste-based ZnO materials as highly efficient photocatalysts for water treatment, J. Environ. Chem. Eng. 10 (2) (2022) 107256.

[29] M. Chen, C. Bao, D. Hu, X. Jin, Q. Huang, Facile and low-cost fabrication of ZnO/biochar nanocomposites from jute fibers for efficient and stable photodegradation of methylene blue dye, J. Anal. Appl. Pyrol. 139 (2019) 319–332.

[30] A.S. Abdalrhman, C. Wang, Z.T. How, M. Gamal El-Din, Degradation of cyclohexanecarboxylic acid as a model naphthenic acid by the UV/chlorine process: Kinetics and by-products identification, J. Hazard. Mater. 402 (2021) 123476.

[31] J. Song, Z.T. How, Z. Huang, M. Gamal El-Din, Biochar/iron oxide composite as an efficient peroxymonosulfate catalyst for the degradation of model naphthenic acids compounds, Chem. Eng. J. 429 (2022) 132220.

[32] S.M. Shaheen, N.K. Niazi, N.E.E. Hassan, I. Bibi, H. Wang, D.C.W. Tsang, Y.S. Ok, N. Bolan, J. Rinklebe, Wood-based biochar for the removal of potentially toxic elements in water and wastewater: a critical review, Int. Mater. Rev. 64 (4) (2019) 216–247.

[33] M. He, Z. Xu, Y. Sun, P.S. Chan, I. Lui, D.C.W. Tsang, Critical impacts of pyrolysis conditions and activation methods on application-oriented production of wood waste-derived biochar, Bioresour. Technol. 341 (2021) 125811.

[34] P. Boguta, Z. Sokołowska, K. Skic, A. Tomczyk, Chemically engineered biochar – Effect of concentration and type of modifier on sorption and structural properties of biochar from wood waste, Fuel 256 (2019) 115893.

[35] Y.L. Pang, Z.X. Law, S. Lim, Y.Y. Chan, S.H. Shuit, W.C. Chong, C.W. Lai, Enhanced photocatalytic degradation of methyl orange by coconut shell–derived biochar composites under visible LED light irradiation, Environ. Sci. Pollut. Res. 28 (21) (2021) 27457–27473.

[36] V.-T. Nguyen, T.-D.-H. Vo, T.-B. Nguyen, N.D. Dat, B.T. Huu, X.-C. Nguyen, T. Tran, T.-N.-C. Le, T.-G.-H. Duong, M.-H. Bui, C.-D. Dong, X.-T. Bui, Adsorption of norfloxacin from aqueous solution on biochar derived from spent coffee ground: Master variables and response surface method optimized adsorption process, Chemosphere 288 (2022) 132577.

[37] H.M. Jang, S. Yoo, Y.-K. Choi, S. Park, E. Kan, Adsorption isotherm, kinetic modeling and mechanism of tetracycline on Pinus taeda-derived activated biochar, Bioresour. Technol. 259 (2018) 24–31.

[38] I. Sánchez-Montes, H. Mokarizadeh, S. Paul, K. Moghrabi, N. Hussain, P. Chelme-Ayala, J.L. Stafford, M.R.V. Lanza, M. Gamal El-Din, UVA LED-assisted breakdown of persulfate oxidants for the treatment of real oil sands process water: Removal of naphthenic acids and evaluation of residual toxicity, Chem. Eng. J. 481 (2024) 148631.

[39] M.A. Suara, S.O. Ganiyu, S. Paul, J.L. Stafford, M.G. El-Din, Solar-activated zinc oxide photocatalytic treatment of real oil sands process water: Effect of treatment parameters on naphthenic acids, polyaromatic hydrocarbons and acute toxicity removal, Sci. Total Environ. 819 (2022) 153029.

[40] S.M. Miles, E. Asiedu, A.-L. Balaberda, A.C. Ulrich, Oil sands process affected water sourced Trichoderma harzianum demonstrates capacity for mycoremediation of naphthenic acid fraction compounds, Chemosphere 258 (2020) 127281.

[41] A. Kamal, M.H. Saleem, H. Alshaya, M.K. Okla, H.J. Chaudhary, M.F.H. Munis, Ball-milled synthesis of maize biochar-ZnO nanocomposite (MB-ZnO) and estimation of its photocatalytic ability against different organic and inorganic pollutants, J. Saudi Chem. Soc. 26 (3) (2022) 101445.

[42] M. Amir, T. Fazal, J. Iqbal, A.A. Din, A. Ahmed, A. Ali, A. Razzaq, Z. Ali, M.S. U. Rehman, Y.-K. Park, Integrated adsorptive and photocatalytic degradation of pharmaceutical micropollutant, ciprofloxacin employing biochar-ZnO composite photocatalysts, J. Ind. Eng. Chem. 115 (2022) 171–182.

[43] M. Choi, C. Brabec, T. Hayakawa, X-ray diffraction, micro-Raman and X-ray photoemission spectroscopic investigations for hydrothermally obtained hybrid compounds of delafossite CuGaO2 and Wurtzite ZnO, Ceramics 5 (4) (2022) 655–672.

[44] R. Al-Gaashani, S. Radiman, A.R. Daud, N. Tabet, Y. Al-Douri, XPS and optical studies of different morphologies of ZnO nanostructures prepared by microwave methods, Ceram. Int. 39 (3) (2013) 2283–2292.

[45] N. Joshi, L.F. da Silva, F.M. Shimizu, V.R. Mastelaro, J.-C. M'Peko, L. Lin, O. N. Oliveira, UV-assisted chemiresistors made with gold-modified ZnO nanorods to detect ozone gas at room temperature, Microchim. Acta 186 (7) (2019) 418.

[46] S.J. Park, G.S. Das, F. Schütt, R. Adelung, Y.K. Mishra, K.M. Tripathi, T. Kim, Visible-light photocatalysis by carbon-nano-onion-functionalized ZnO tetrapods: degradation of 2,4-dinitrophenol and a plant-model-based ecological assessment, NPG Asia Mater. 11 (1) (2019) 8.

[47] H. Jing, L. Ji, Z. Wang, J. Guo, S. Lu, J. Sun, L. Cai, Y. Wang, Synthesis of ZnO nanoparticles loaded on biochar derived from spartina alterniflora with superior photocatalytic degradation performance, Nanomaterials 11 (10) (2021) 2479.

[48] C.H. Kim, B.-H. Kim, Zinc oxide/activated carbon nanofiber composites for high-performance supercapacitor electrodes, J. Power Sources 274 (2015) 512–520.

[49] Y. He, Y. Wang, J. Hu, K. Wang, Y. Zhai, Y. Chen, Y. Duan, Y. Wang, W. Zhang, Photocatalytic property correlated with microstructural evolution of the biochar/ZnO composites, J. Mater. Res. Technol. 11 (2021) 1308–1321.

[50] Mankomal, and Kaur, H. 2022. Synergistic effect of biochar impregnated with ZnO nano-flowers for effective removal of organic pollutants from wastewater. Appl. Surf. Sci. Adv. 12: 100339.

[51] L. Li, L. Liu, Z. Li, D. Hu, C. Gao, J. Xiong, W. Li, The synthesis of CB[8]/ZnO composites materials with enhanced photocatalytic activities, Heliyon 5 (5) (2019) e01714.

[52] A.C. Ekennia, D.N. Uduagwu, N.N. Nwaji, O.O. Oje, C.O. Emma-Uba, S.I. Mgbii, O. J. Olowo, O.L. Nwanji, Green synthesis of biogenic zinc oxide nanoflower as dual agent for photodegradation of an organic dye and tyrosinase inhibitor, J. Inorg. Organomet. Polym Mater. 31 (2) (2021) 886–897.

[53] P. Makuła, M. Pacia, W. Macyk, How to correctly determine the band gap energy of modified semiconductor photocatalysts based on UV–Vis spectra, J. Phys. Chem. Lett. 9 (23) (2018) 6814–6817.

[54] A. Afzal, P. Chelme-Ayala, P. Drzewicz, J.W. Martin, M. Gamal El-Din, Effects of ozone and ozone/hydrogen peroxide on the degradation of model and real oil-sands-process-affected-water naphthenic acids, Ozone Sci. Eng. 37 (1) (2015) 45–54.

[55] A.B. Makama, A. Salmiaton, T.S.Y. Choong, M.R.A. Hamid, N. Abdullah, E. Saion, Influence of parameters and radical scavengers on the visible-light-induced degradation of ciprofloxacin in ZnO/SnS2 nanocomposite suspension: Identification of transformation products, Chemosphere 253 (2020) 126689.

[56] E. Braxton, D.J. Fox, B.G. Breeze, J.J. Tully, K.J. Levey, M.E. Newton, J. V. Macpherson, Electron paramagnetic resonance for the detection of electrochemically generated hydroxyl radicals: issues associated with electrochemical oxidation of the spin trap, ACS Meas. Sci. Au 3 (1) (2023) 21–31.

[57] S.O. Ganiyu, M. Arslan, M. Gamal El-Din, Combined solar activated sulfate radical-based advanced oxidation processes (SR-AOPs) and biofiltration for the remediation of dissolved organics in oil sands produced water, Chem. Eng. J. 433 (2022) 134579.

[58] M. Antonopoulou, P. Bika, I. Papailias, S.-K. Zervou, A. Vrettou, I. Efthimiou, G. Mitrikas, N. Ioannidis, C. Trapalis, P. Dallas, D. Vlastos, A. Hiskia, Photocatalytic degradation of organic micropollutants under UV-A and visible light irradiation by exfoliated g-C3N4 catalysts, Sci. Total Environ. 892 (2023) 164218.

[59] K.M. Lee, C.W. Lai, K.S. Ngai, J.C. Juan, Recent developments of zinc oxide based photocatalyst in water treatment technology: A review, Water Res. 88 (2016) 428–448.

[60] Y. Li, Q. Lu, M. Gamal Ei-Din, X. Zhang, Immobilization of photocatalytic ZnO nanocaps on planar and curved surfaces for the photodegradation of organic contaminants in water, ACS ES&T Water 3 (8) (2023) 2740–2752.

[61] F. Jahani, B. Maleki, M. Mansouri, Z. Noorimotlagh, S.A. Mirzaee, Enhanced photocatalytic performance of milkvetch-derived biochar via ZnO–Ce nanoparticle decoration for reactive blue 19 dye removal, Sci. Rep. 13 (1) (2023) 17824.

[62] D. de Oliveira Livera, T. Leshuk, K.M. Peru, J.V. Headley, F. Gu, Structure-reactivity relationship of naphthenic acids in the photocatalytic degradation process, Chemosphere 200 (2018) 180–190.

[63] A. Afzal, P. Drzewicz, L.A. Pérez-Estrada, Y. Chen, J.W. Martin, M. Gamal El-Din, Effect of molecular structure on the relative reactivity of naphthenic acids in the UV/H2O2 advanced oxidation process, Environ. Sci. Tech. 46 (19) (2012) 10727–10734.

[64] N.W.C. Jusoh, A.A. Jalil, S. Triwahyono, H.D. Setiabudi, N. Sapawe, M.A.H. Satar, A.H. Karim, N.H.N. Kamarudin, R. Jusoh, N.F. Jaafar, N. Salamun, J. Efendi, Sequential desilication–isomorphous substitution route to prepare mesostructured silica nanoparticles loaded with ZnO and their photocatalytic activity, Appl. Catal. A 468 (2013) 276–287.

[65] USEPA. 2007. National Recommended Water Quality Criteria - Aquatic Life Criteria Table. *Edited by* U.S.E.P. Agency.